Shock Waves (2015) 25:623–633
DOI 10.1007/s00193-015-0595-y

ORIGINAL ARTICLE

Unsteady transitions of separation patterns in single expansion ramp nozzle

Y. Yu[1] · J. Xu[1] · K. Yu[1] · J. Mo[1]

Received: 19 February 2014 / Revised: 20 July 2015 / Accepted: 20 August 2015 / Published online: 21 September 2015

Abstract The single expansion ramp nozzle is one of the optimal configurations for a planar rocket-based combined cycle engine because of its good integration and self-adaptability at off-design operation. The single expansion ramp nozzle is seriously overexpanded when the vehicle is at low speed, resulting in complex flow separation phenomena. Several separation patterns have been found in the single expansion ramp nozzle. Numerical simulations have shown that the transition between these separation patterns occurs in the nozzle startup and shutdown processes. However, only a few relevant experimental studies have been reported. This study reproduces the nozzle startup and shutdown processes using wind tunnel experiments. Two restricted shock separation patterns are observed in the experiment, namely, a separation bubble either forms on the ramp or the flap. The detailed flow fields in the transition processes are captured using a high-speed camera. The shock wave structures in the two separation patterns, influences of the nozzle pressure ratio (NPR) on the separation patterns and changes of the shock waves in the transition processes are discussed in detail. Shock wave instabilities accompany the separation transition, which usually takes less than 5 ms. The nozzle pressure ratios corresponding to the separation pattern transition are different in the startup and shutdown processes, which leads to a hysteresis effect.

Keywords SERN · Flow separation · Shock wave · Transition · Hysteresis

1 Introduction

A vehicle cannot take off from the ground and accelerate to hypersonic cruise or orbit using a propulsion system such as a turbojet, turbofan, ramjet or scramjet engine. Hence, combined cycle propulsion systems are required for hypersonic vehicles that take off from the ground and cruise at a high Mach number [1]. The combined cycle engines are comprised of different engines, taking advantage of the merits of each technology to maintain high performance in a wide range of flight Mach numbers. Among these engines, the rocket-based combined cycle (RBCC) and turbine-based combined cycle (TBCC) engines have attracted much attention. The RBCC engine generally has four operating modes: ejector-jet, ramjet, scramjet and rocket. The ejector-jet mode operates in the range of Mach 0–3, the ramjet mode operates in the range Mach 3–7, whilst the scramjet and rocket modes operate at Mach numbers 7–11 and higher than 11, respectively [2]. The RBCC engine can be a fixed geometry configuration using thermal throat, which avoids a complex and heavy controlling device, thereby reducing engine weight [3].

The nozzle pressure ratio (NPR, i.e., the ratio of internal total pressure at the nozzle entrance to the static ambient pressure) of the RBCC engine ranges from 2 at low Mach numbers, up to 600 (or even higher) for hypersonic flight [4]. The RBCC engine requires varying nozzle expansion area ratios, which imposes high demands on the design of the exhaust system. A promising candidate that fulfills these challenging requirements of high performance over a wide operating range of Mach numbers is the single expansion ramp nozzle (SERN). The SERN has good integration and self-

Communicated by A. Hadjadj and G. Ciccarelli.

✉ J. Xu
xujl@nuaa.edu.cn

[1] Jiangsu Province Key Laboratory of Aerospace Power System, Nanjing University of Aeronautics and Astronautics, Nanjing 210016, People's Republic of China

adaptability at off-design conditions [5]. However, the performance of SERN at relatively low Mach numbers is greatly influenced by unavoidable flow separation [6]. The flow through the nozzle is overexpanded during a low Mach number flight, which results in a low pressure acting on the expansion ramp. Sub-ambient exhaust pressures tend to increase drag and reduce performance. These adverse effects cause as much as 25 % reduction in the net thrust-minus-drag performance [7]. Flow separation occurs, and shock wave boundary layer interaction (SWBLI) may induce highly unsteady flow conditions in highly overexpanded nozzles, including the rocket axisymmetric thrust nozzle [8]. These effects are undesirable in the rocket nozzle because the unsteadiness and the asymmetry in the flow produce powerful, statistical lateral forces that could result in damage to the nozzle. These problems have been the focus of research for decades [9].

Shock wave boundary layer interactions usually accompany flow separation in an overexpanded supersonic nozzle. Moreover, flow separation may take on various patterns because the shock waves and the beginning of the separation are different [10]. From a gas dynamics viewpoint, this difference is essentially a problem of shock wave interactions including many complex phenomena (e.g., incident shocks, Mach reflections, reflected shocks, triple points and shear layers) [11]. Various shock reflections might occur in a supersonic nozzle (Fig. 1). If the internal shock impinges with the central Mach disk, the cap shock pattern is formed. The reflected shock and the incident shock may form either a regular reflection or a Mach Reflection. The internal shock can be observed in the nozzles, shortly downstream of the throat, where the curvature changes from a convex to a concave contour. The unsteady flow caused by the SWBLI in an overexpanded nozzle may lead to asymmetric separation in a symmetric configuration. Bourgoing [12] and Papamoschou [13] observed the symmetric and asymmetric separation patterns in planar convergent–divergent nozzles (Fig. 2). Various separation patterns are also found in axisymmetric rocket nozzles. The most typical patterns are free shock separation (FSS) and restricted shock separation (RSS). The FSS pattern is the most common separation pattern in rocket nozzles, which has been reported by many researchers in the early 1950s and 1960s [14]. The FSS pattern was the most investigated pattern until 1973, when the RSS pattern was first confirmed in cold-flow subscale tests of the J-2S engine [15]. The separation pattern transitions in the startup and shutdown processes were observed in the testing of the LE-7A engine [16]. Irregular lateral forces also accompanied the separation, and the maximum lateral force was found during the separation pattern transition. The powerful lateral forces damaged the nozzle, and some regenerative cooling tubes were broken in the startup and shutdown transients during the test.

Similar to the rocket nozzle, various separation patterns and transitions were found in the startup and shutdown processes for the SERN. Yu et al. [17] observed two separation patterns and transitions in cold-flow subscale SERN tests. They investigated the transition processes using computational fluid dynamics. The sketches of the two separation patterns [i.e., RSS with the separation bubble forming on the expansion ramp or RSS(ramp) and on the flap or RSS(flap)] based on the numerical results in Ref. [17], and the current understanding of the flow fields, are shown in Fig. 3. The flow in the RSS(ramp) separates both from the expansion ramp and the flap but reattaches to the expansion ramp, forming a separation bubble. A normal shock wave, or Mach disk (MD) forms in the SERN, and two typical "λ" shock structures form as a result of the interaction of two separation shock waves

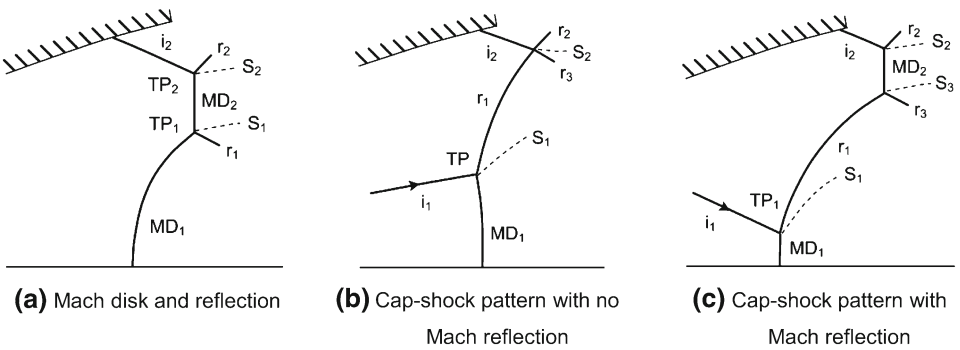

Fig. 1 Shock interactions in overexpanded rocket nozzles (reproduced from [11]), *i* incident shock, *r* reflected shock, *MD* Mach disk, *TP* triple point, *S* slip-line

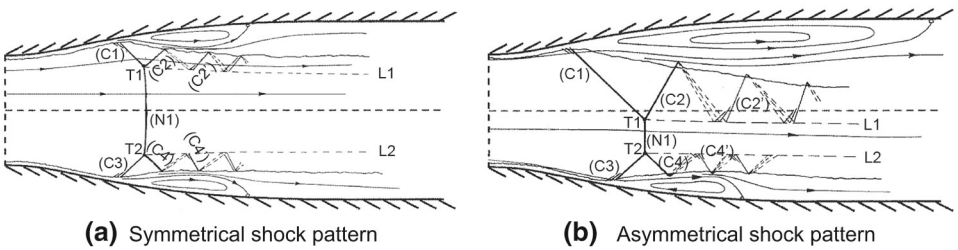

Fig. 2 Various separated patterns in a supersonic planar nozzle (reproduced from [12]), *C* oblique shock, *N* normal shock, *T* triple point, *L* slip-line

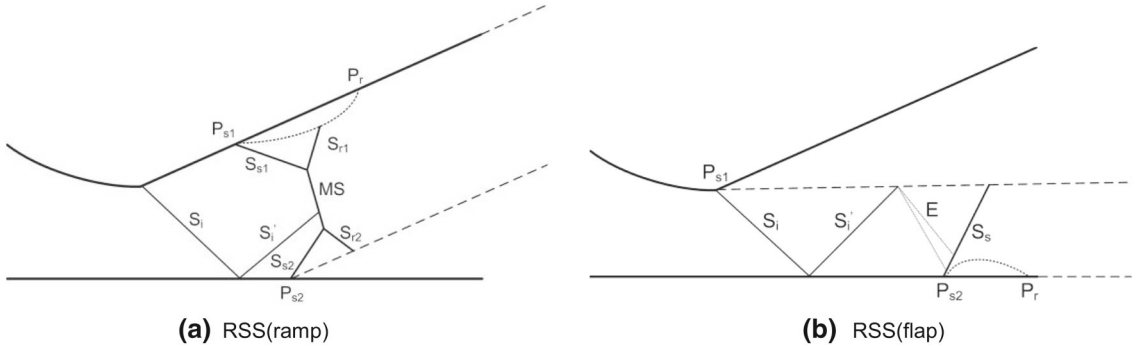

Fig. 3 Sketches of the separation patterns in the SERN, S_i internal shock, S_i' reflected shock of S_i, S_s separation shock, S_r reflected shock, P_s separation point, P_r reattachment point, *MS* Mach stem, *E* expansion fan, *the dotted line* slip-line

(i.e., S_{S1} and S_{S2}). The internal shock (S_i) of the RSS(flap), which is created by the curvature change between the rounded throat and the straight expansion ramp, is stronger than that in the RSS(ramp). This internal shock affects the entire downstream flow structure. A separation shock (S_S) is formed on the flap, that is followed by a separation bubble downstream. The numerical results demonstrate that the separation pattern transition is completed within a short period of time. Moreover, the thrust, lift and moment of the nozzle abruptly change during the transition. These changes in the performance pose a great challenge for the aerodynamic control and durability of the SERN [17].

The complex flow separation in the SERN is a key problem. However, the separation patterns and the phenomena that accompany the transition of the separation patterns have not attracted much attention from researchers. The flow separation experienced by the SERN at low flight speeds has not been fully addressed. Furthermore, the detailed process and separation patterns of flow separation, the dynamic mechanics of the separation pattern transition and the effect on the performance have not been investigated. More importantly, little experimental data on the details of the dynamic process of the flow separation have been reported in the literature. Therefore, the experimental study of the flow separation and separation pattern transitions in the SERN is a critical problem that needs to be addressed.

This study reproduces the startup and shutdown processes of the SERN using wind tunnel experiments. Two separation patterns are observed in the experiment. The detailed flow field during the transition process is captured using schlieren photography. The influence of the NPR on the two separation patterns observed is discussed in detail.

2 Apparatus and experiment

The experiments were conducted at the Internal Flow Research Center of Nanjing University of Aeronautics and Astronautics. The facility utilized a cold blow-down wind tunnel [18]. The test air was supplied from a high-pressure vessel, with a maximum stagnation pressure ranging from 0.8 to 0.9 MPa. The low back pressure was generated by vacuum pumps, and the minimum back pressure ranged from 3 to 5 kPa. The maximum mass flow rate was 0.8 kg/s. The test system included a schlieren system that included a high-resolution, high-speed camera and a pressure scanning system. Figure 4 provides a sketch of the wind tunnel. The schlieren system was a Z-type system, with 200 mm diameter concave mirrors. Standard schlieren photo and video were taken using a Canon 500D camera. The maximum photo resolution was 4752 × 3168 pixels, whilst the maximum video resolution was 1920 × 1080 pixels at a speed of 20 fps. The high-speed camera used was an IDT MotionPro Y5. The maximum camera resolution was 2336 × 1728 pixels at a speed of 730 fps. The maximum speed achievable was 69,000 fps with 2336 × 16 pixels. The precision of the sensors used in the pressure scanning system was 0.05 % of the full scale.

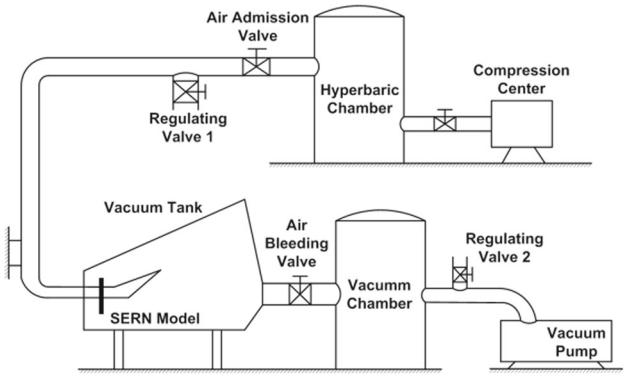

Fig. 4 Sketch of the wind tunnel

The test model was a subscale planar SERN (Fig. 5) similar to the long flap SERN model simulated in Ref. [17]. The model contained a straight expansion ramp with a 25° expansion angle. The expansion area ratio was 2.896, and the throat

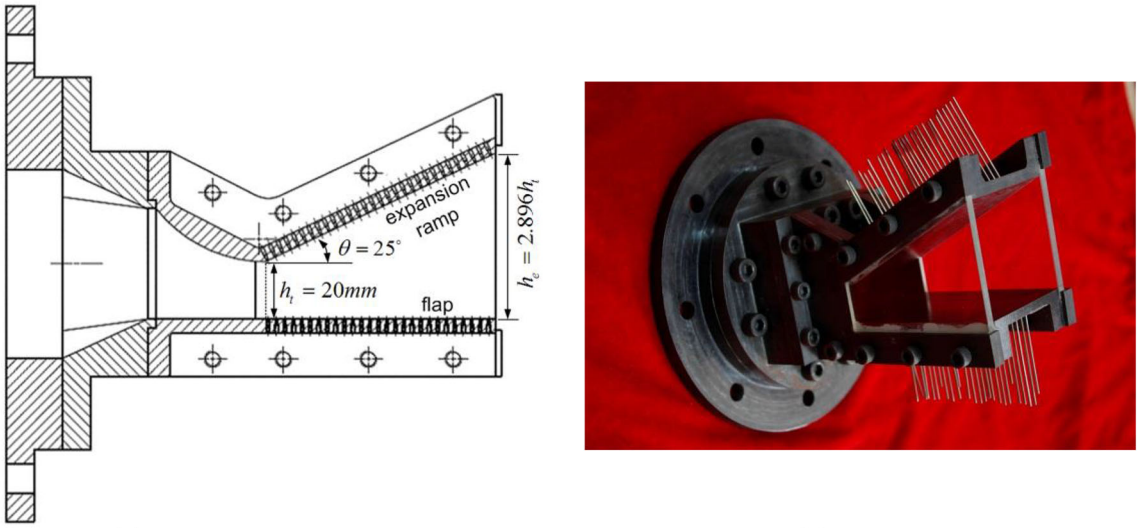

(a) SERN model configuration **(b)** SERN model

Fig. 5 SERN model tested in the experiment

area was 1200 mm^2. The length of the flap, which was 60 mm wide, was similar to the length of the expansion ramp. The sidewalls of the nozzle were made of optical glass to facilitate schlieren observation of the model's internal flow field. A 30-mm-long transition section was used between the round and the rectangular sections. Accordingly, the diameter of the round transition was 66 mm and that of the rectangular transition was 60 × 38.5 mm. The transition surface was a ruled surface generated in the software package UGS NX. The ruled surface can be formed as a set of points swept by a moving straight line. The unit Reynolds number based on the 575 m s^{-1} exit velocity was about 5×10^6 m^{-1}. The pipe system before the entrance of the SERN is complex, which will disturb the boundary layers. Moreover, the wall of the round-to-rectangle transition and the contraction part of the SERN are roughened by sandpaper to promote the incoming boundary layers' transition. The surface roughness Ra, as arithmetic average of absolute deviations, is about 100 μm. Therefore, the boundary layers are turbulent where separation occurred.

The startup and shutdown processes in the experiment were simulated by increasing and decreasing the NPR, which was achieved by continuously and steadily adjusting the back pressure.

3 Results and discussions

3.1 NPR

The pressure in the vacuum chamber at the beginning of the experiment was similar to the atmospheric pressure. Subsequently, the vacuum pumps were operated, and the back pressure P_b of the SERN gradually dropped. However, the total pressure P_c at the SERN inlet was kept constant because the air was sucked from the atmosphere. Hence, the NPR of the SERN increased steadily and continuously, simulating the startup process. The transition from one separation pattern to another was completed when the NPR reached about 3.0. The shutdown process was initiated by turning off the vacuum pumps, in which case the ambient air was sucked into the vacuum chamber through the SERN. Consequently, the back pressure increased, and the NPR of the nozzle gradually decreased. The experiment was considered finished when the NPR was lower than 2.0.

Two separation patterns [i.e., RSS(ramp) and RSS(flap)] were observed when the SERN was operated under a highly overexpanded condition. The transition of the separation patterns occurred during the startup and the shutdown processes. The NPR abruptly changed after the transition because the operating condition of the tunnel was different for the various separation patterns. The jet flowed along the flap and the airstream flowed out of the vacuum tank smoothly when the SERN operated under RSS(flap). The jet flowed along the expansion ramp and the air did not flow directly to the vacuum tank exit when the nozzle operated under RSS(ramp). Consequently, the back pressure of the SERN increased after the RSS(flap) transition to RSS(ramp) and decreased after RSS(ramp) transition to RSS(flap). The measured total pressure at the inlet and back pressure provided a critical NPR of 2.95 and 2.28 in the startup and the shutdown processes, respectively (Fig. 6).

3.2 RSS with the separation bubble forming on the ramp

The most common separation pattern in the SERN was the RSS. The flow in the RSS reattached to the wall downstream from the separation point and formed a closed separation

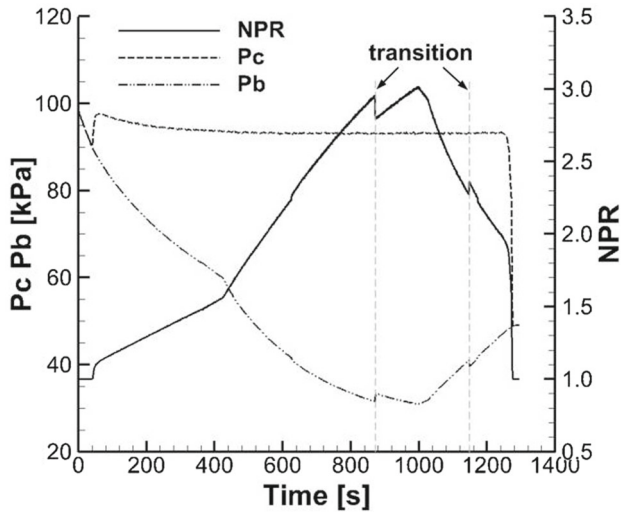

Fig. 6 Total pressure P_c at the inlet, back pressure P_b and NPR

bubble. The separation bubble could form on the expansion ramp or on the SERN flap. The expansion ramp was the most important contour, in which the flow rapidly expanded. Hence, the separation bubble formed more easily on the ramp than on the flap. The RSS(ramp) was obtained in many experimental and numerical results [17]. The RSS(ramp) in this experiment was obtained using the schlieren system, and the flow field was similar to that in the numerical results. Figure 7 presents the main shock wave structures. However, the Mach number after the reflected shock was so low that the shock train was not detected by the schlieren system. The detailed structure came from the numerical simulation results in Ref. [17]. The flow could also separate from both the ramp and the flap. However, unlike the symmetric rocket nozzle, the SERN was inherently asymmetric because the air expanded primarily on the expansion ramp. The position of the separation points and the strength of the separation shock waves were different in the expansion ramp and the flap.

The Mach number and the flow direction in front of the separation shock waves were different. Hence, the separation shock waves were curved. The Mach numbers in front of the separation point on the expansion ramp and the flap were about 2 and 1.8, respectively. The Mach number in front of the separation shock waves near the Mach stem was about 2.1. The normal shock wave in the SERN was caused by the interaction of the two separation shock waves. Furthermore, the typical "λ" shock structures were formed by the intersection and reflection of the separation shock waves and the normal shock waves. The flow reattached downstream from the separation point on the expansion ramp, and a closed separation bubble formed between the separation and the reattachment points. A series of shock waves, expansion waves and compression waves was generated downstream from the reattachment to match the back pressure. The number of waves depended on the separation point position and the operating NPR. The separation shock and the normal shock on the expansion ramp intersected, and a reflected shock was consequently generated. This shock wave affected the separation bubble boundary, and a set of expansion waves was reflected. The expansion waves intersected with the subsonic region boundary and were reflected as compression waves. The waves were subsequently reflected on the expansion ramp and the slip-line. The pressure downstream from the reflected shock was higher than that downstream from the normal shock. Consequently, an expansion fan was found emerging from the triple point. The expansion waves affected the separation bubble and were reflected as compression waves. The compression waves merged with the shock waves generated by the reattachment and were reflected on the expansion ramp and the slip-line. These waves composed the wave train on the expansion ramp downstream the separation shock. The flow on the flap did not reattach to the wall, and no separation bubble was formed. Therefore, the flow was not influenced by the wall, and the waves were reflected only at the jet boundary. The aerodynamic boundaries were deflected because of the intersection of the expansion and compression waves. The slip-lines of the subsonic flow formed a convergent–divergent flow path, and as a result the subsonic flow was alternately accelerated and decelerated.

Figure 8 shows the shock wave structures at different NPRs. The circle, square and triangle markers denote the separation point on the expansion ramp, the triple point and

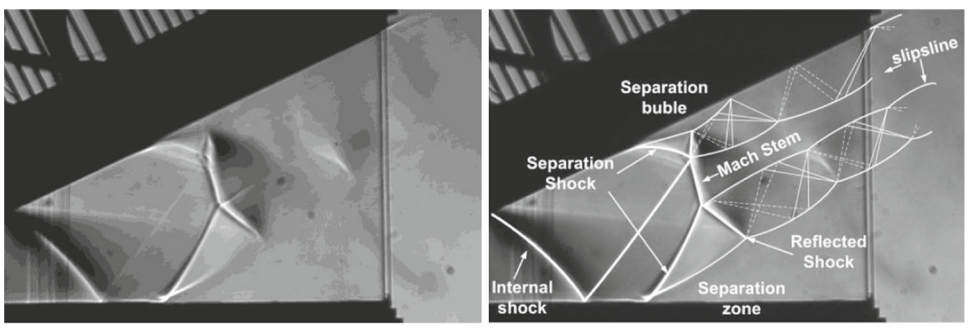

Fig. 7 Shock wave structure in the RSS(ramp) mode: NPR = 2.85

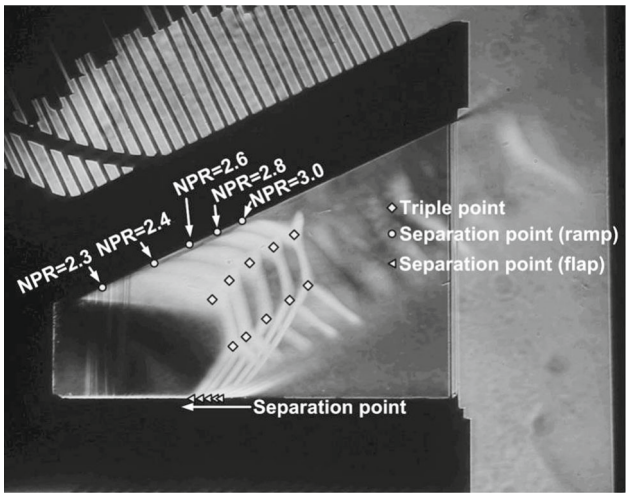

Fig. 8 Shock wave structure in different NPRs: RSS(ramp)

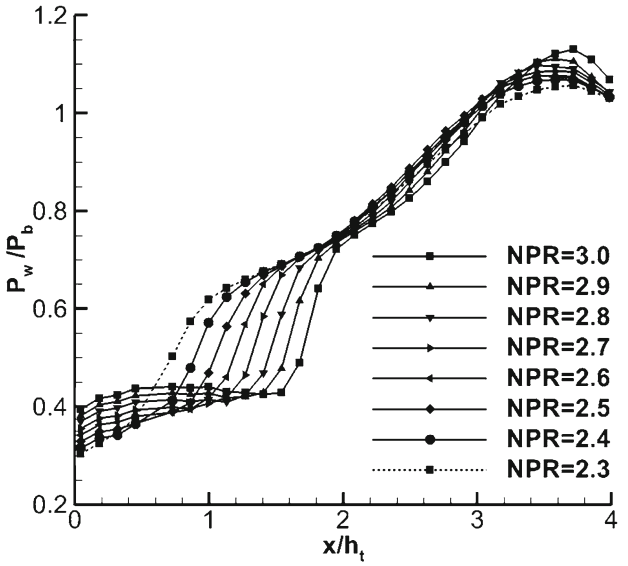

Fig. 9 Pressure distributions on the centreline of the expansion ramp in different NPRs: RSS(ramp)

the separation point on the flap, respectively. The approximate (to be discussed below) separation locations are shown. The separation point on the expansion ramp was sensitive to the NPR. The separation shock angle on the expansion ramp decreased with the decrease of the NPR. The NPR had minimal influence on the separation point and shock strength on the flap. The separation point moved a little, and the separation shock angle remained almost constant when the NPR was decreased. The separation shock abruptly increased the pressure downstream. The sudden increase in pressure was used to identify the separation point. Determining the separation point in the experiment precisely was difficult. However, tit was useful to identify trends. From the measured pressure distributions on the centreline of the expansion ramp, the position of the pressure increase and the separation point both moved upstream (Fig. 9) with the decrease in the NPR. The maximum pressure caused by the wave train was higher than the back pressure.

The separation point moved a little based on the measured pressure distribution P_w on the centreline of the flap. This change in position was in agreement with the schlieren results. P_w/P_c under an NPR of 2.4 was higher than that under an NPR of 2.5 for the fourth point from the throat (Fig. 10a). This result was obtained because the point was before the separation shock when the NPR was 2.5 and was behind and closer to the separation shock when the NPR was 2.4. This reaction caused the increase in pressure. Therefore, the separation point under an NPR of 2.4 was closer to the throat than that under an NPR of 2.5. P_w/P_c under an NPR of 2.3 was much higher than that under other NPRs because the point was on the separation shock. Accordingly, this position caused the abrupt increase in pressure. The separation point under an NPR of 2.3 was closest to the throat. P_w/P_b under an NPR of 3.0 was a little lower than that in the separation zone for the fifth point from the throat (Fig. 10b), because the point was at the tail of the separation shock and the pressure did not fully increase. Therefore, the separation point under an NPR of 3.0 was the farthest from the throat (Fig. 10). The slight change in each NPR suggested that the separation point on the flap moved very little with the varying NPR. The pressure in the separation zone was close to the back pressure because the ambient air entered the separation zone.

3.3 RSS with the separation bubble forming on the flap

The flow separated from both the expansion ramp and the flap. Hence, the reattachment occurred not only on the expansion ramp but also on the flap. The RSS(flap) and the RSS(ramp) were quite different from each other because of the asymmetry of the nozzle configuration. The RSS(flap) in the experiment was captured using the schlieren system. Figure 11 presents the main shock wave structures. The flow separated from the flap and reattached on the flap downstream, which generated a separation shock and formed a separation bubble on the flap. The separation point on the expansion ramp, which was distinguished from the numerical results of the RSS(flap) in Ref. [17], was very close to the throat. Accordingly, the internal shock impinged on the flap. The internal shock deflected the flow towards the flap, and the air stream mainly flowed along the flap. An expansion fan was formed at the throat and reflected on the flap. The internal shock intersected with the expansion fan and bent. The expansion waves crossed the internal shock, intersected the jet boundary and transitioned into compression waves. The compression waves impinged on the flap and formed a shock wave. The strength of the shock wave depended on the Mach number. A separation bubble was formed downstream

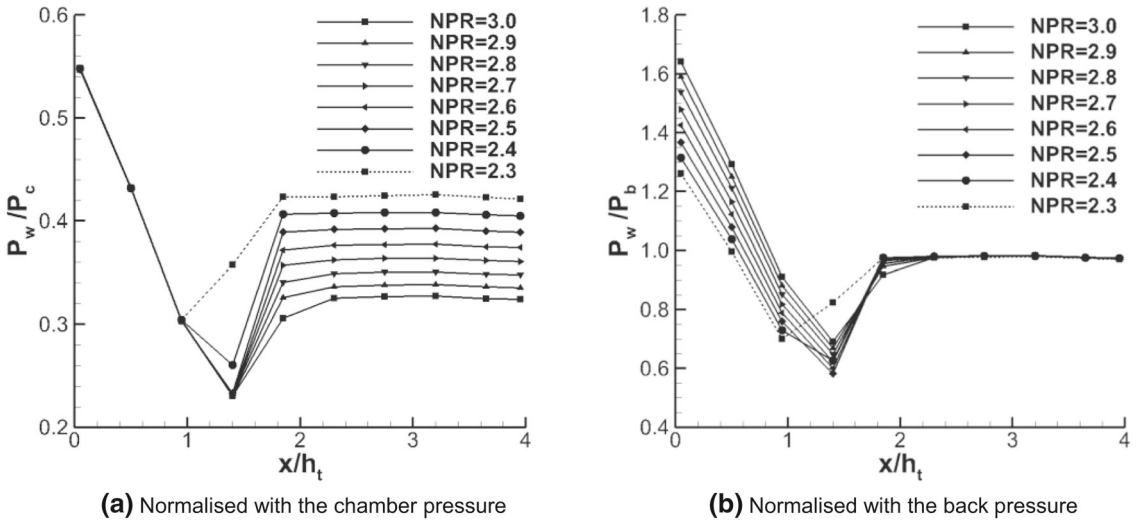

Fig. 10 Pressure distribution on the centreline of the flap in different NPRs: RSS(ramp)

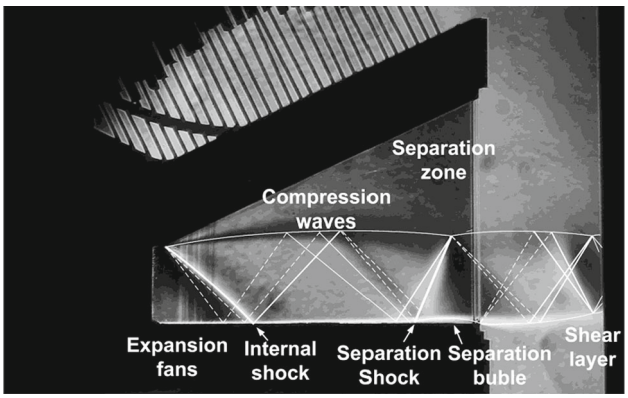

Fig. 11 Shock wave structure under the RSS(flap) mode: NPR = 2.9

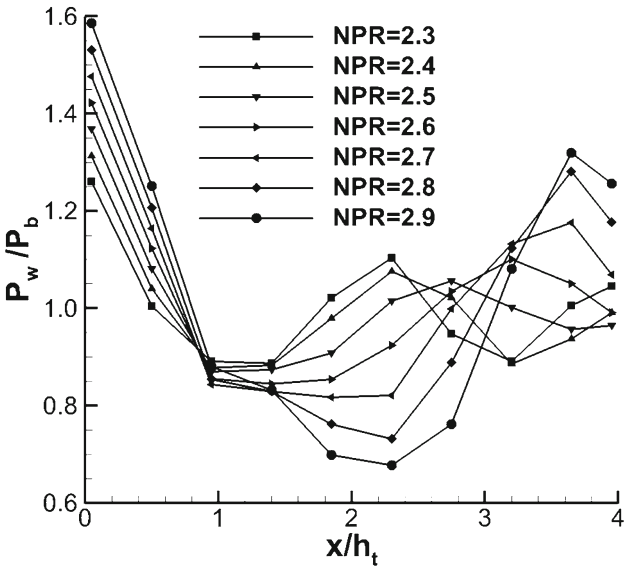

Fig. 12 Pressure distribution on the centreline of the flap in different NPRs: RSS(flap)

the shock wave, and the reattachment took place at the flap tail. Compared with that in the RSS(ramp), the shock wave structure in the RSS(flap) was simpler. Furthermore, the main shock was the separation shock on the flap. Figure 12 shows the pressure distribution P_w on the centreline of the flap. The separation shock wave appeared and the pressure obviously increased when the operating NPR was larger than 2.7. The separation point moved downstream and the separation shock was stronger with the increase in the NPR. The pressure on the expansion ramp was close to the back pressure because the flow separated at the throat and the ambient air entered the separation zone (Fig. 13).

3.4 Transition of the separation pattern in the startup process

The transitions in the separation pattern were observed in the startup and shutdown processes. The jet in the startup process initially flowed along the flap [i.e., RSS(flap) separation pattern] and suddenly switched in the direction along the expansion ramp when the nozzle operated at the critical NPR. Furthermore, the separation pattern transitioned into the RSS(ramp). The transition of the separation pattern was successfully captured by the camera operating at 1560 fps. Figure 14 shows eight typical frames during the transition process. The exposure time was 0.424 ms, and the total video time was about 7.92 s.

The separation shock was not stable and moved upstream at the beginning of the transition process. The separation bubble on the flap became larger and opened-up to the ambient flow when the separation shock moved to the critical position and transferred to a separation zone with the entrainment of the ambient air. The separation shock on the flap during

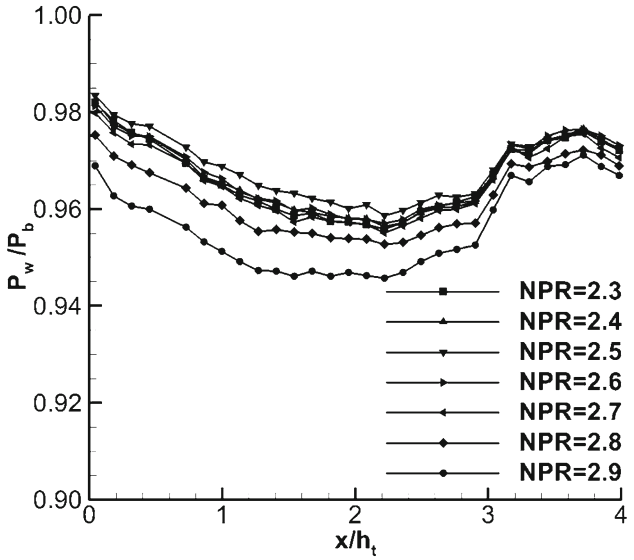

Fig. 13 Pressure distribution on the centreline of the expansion ramp in different NPRs: RSS(flap)

this time was a typical oblique shock wave. The flow was deflected to the expansion ramp downstream of the separation shock. The air then expanded further on the expansion ramp, and a separation shock wave formed. The two separation shock waves interacted with each other and formed two asymmetric λ-type shock wave structures. The shock waves subsequently moved downstream and stabilized. The separation transition process lasted for less than 5 ms according to the high-speed schlieren video.

The internal shock was one of the main shock waves in the RSS(flap) that affected the entire downstream flow structure. However, this internal shock weakened in the RSS(ramp) because the pressure downstream the shock was lower. This pressure was so low that it was not detected by the schlieren system. The reflected shock was very weak and had only a little influence on the structures downstream when the internal shock intersected with the flap.

3.5 Separation pattern transition in the shutdown process

The separation pattern transition was also captured during the shutdown process. The jet initially flowed along the expansion ramp when the NPR was high [i.e., RSS(ramp) separation pattern]. The jet suddenly switched to flow along the flap, and the separation pattern transitioned when the NPR reached the critical value. The transition of the separation pattern was captured by the high-speed camera. Figure 15 shows eight typical frames during the transition process. The camera speed was 1500 fps with an exposure time of 0.424 ms, and the total video time was 8.232 s.

The separation shock on the expansion ramp was not stable at the beginning of the transition process. The shape and the position of the normal shock continuously changed because of oscillations of the separation shock on the expansion ramp. The separation point was close to the throat (because the NPR was low) and the separation shock instantly disappeared when the separation point moved towards the throat. The jet separated at the throat and ambient air entered the separation zone after the separation shock disappeared. This reaction produced a larger force on the jet upper boundary than that on the jet lower boundary and as a result the jet was deflected to the flap. The separation shock on the flap was still present and more fully developed during this point because no constraint of the separation shock was present on the expansion ramp. The separation shock then gradually disappeared, and the flow field became stable. The separation transition process lasted for less than 5 ms. The jet separated at the throat after the transition because the transition NPR was low. Furthermore, the internal shock and the expansion and compression waves formed in the flow field were too weak to be clearly observed by the schlieren system.

3.6 Hysteresis in the separation pattern transitions

The analysis of the transition of separation patterns showed that the instability of the separation shock accompanied the transition of the separation patterns. However, the separation pattern transition and shock appearance/disappearance needed harsh conditions. The critical NPRs of the separation pattern transition during the startup and the shutdown processes were different. Accordingly, the NPR was 2.95 and 2.28 in the startup and the shutdown processes, respectively (Fig. 5). The separation patterns produced during the startup and the shutdown processes were not fixed because the NPRs were different which may be caused by the different shock wave reflection transition criteria [19]. Both the RSS(ramp) and the RSS(flap) may occur in the NPR range from 2.28 to 2.95. In addition, a hysteresis effect was observed in the startup and shutdown processes. Figure 16 shows the relationship of the NPR of the SERN with the separation point on the expansion ramp in the startup and the shutdown processes.

The flow in the RSS(flap) separated at the throat on the expansion ramp. Hence, the position of the separation point was close to 0. The critical transition NPR during the startup process was higher than that in the shutdown process. Hence, the RSS(flap) had a larger range of NPR in the startup process, and the separation point on the expansion ramp moved a longer distance in the transition of RSS(ramp) to RSS(flap). The separation on the expansion ramp rapidly moved downstream during the transition process from RSS(flap) to RSS(ramp). Moreover, an obvious separation bubble was formed on the expansion ramp.

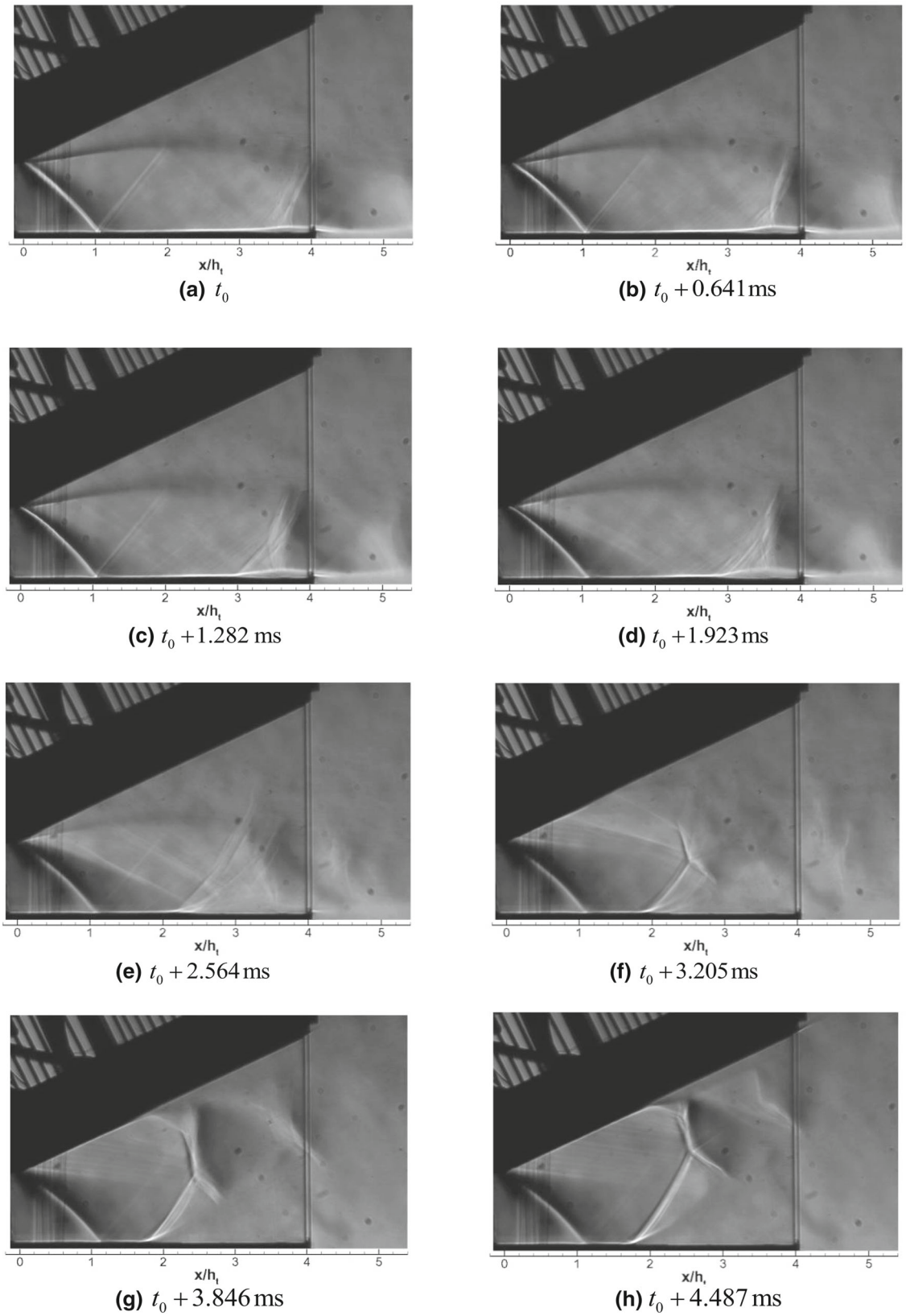

Fig. 14 Transition of the RSS(flap) to the RSS(ramp) captured by the high-speed camera

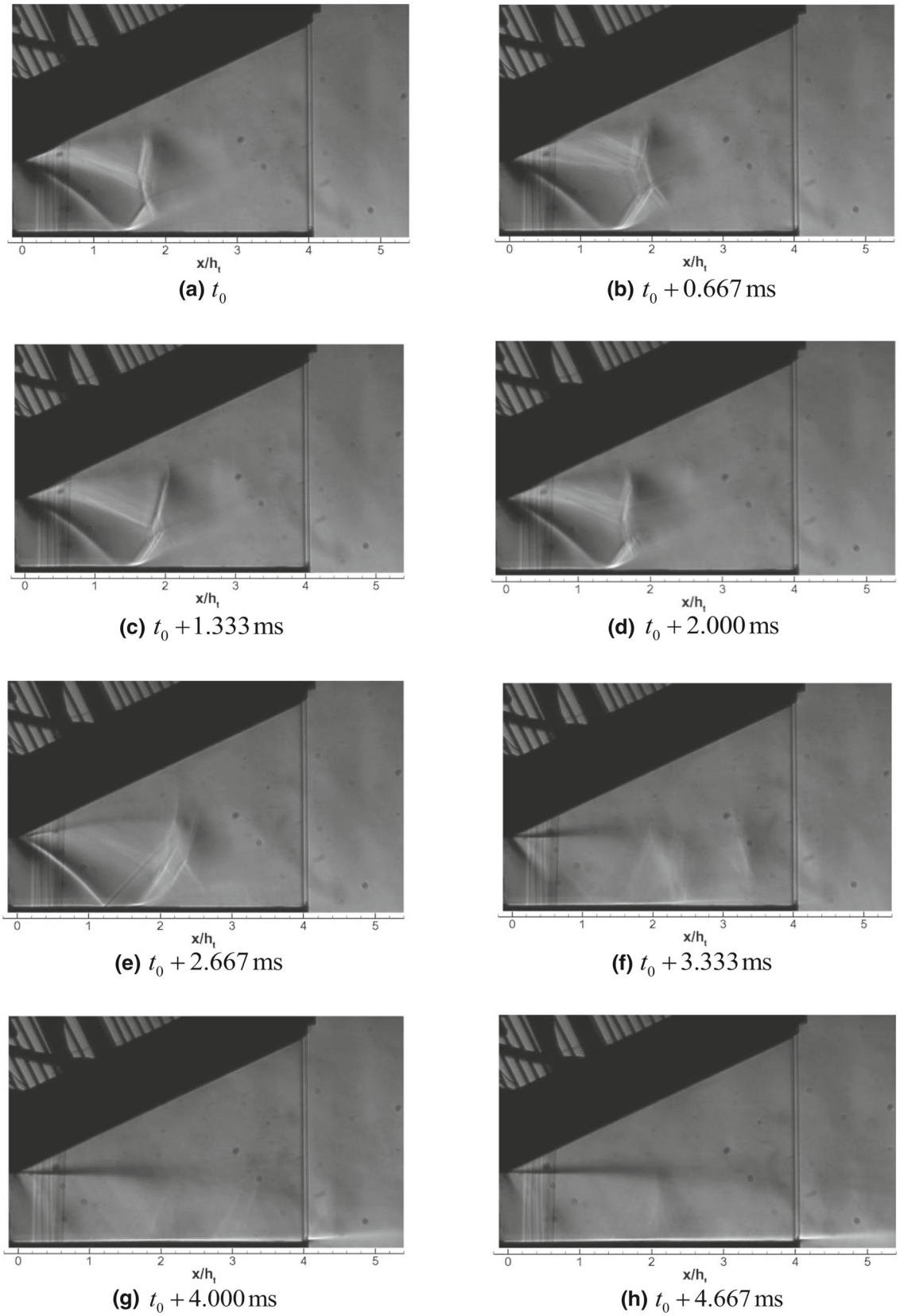

Fig. 15 Transition of the RSS(ramp) to the RSS(flap) captured by the high-speed camera

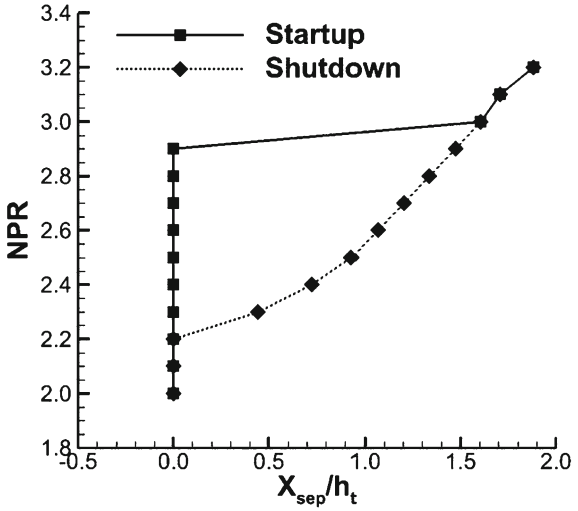

Fig. 16 Separation point on the expansion ramp in the startup and the shutdown processes

The critical NPR was 2.28 during the transition process from RSS(ramp) to RSS(flap). This value was quite low, and the separation point was close to the throat. Consequently, the separation point did not move very far in this transition.

4 Conclusions

This experimental study describes the separation patterns and transitions from one pattern to the other in the subscale SERN model. The following conclusions are drawn from the experimental results:

(a) Two separation patterns have been observed, e.g., RSS (ramp) and RSS(flap). The critical NPR of the RSS-(ramp) is higher than that of the RSS(flap). The pattern transition from the RSS(flap) to the RSS(ramp) occurs during the startup process, whereas during the shutdown process there is a transition from the RSS(ramp) to the RSS(flap).
(b) The position of the separation point on the ramp under the RSS(ramp) condition is sensitive to the NPR. However, the separation point on the flap moves only very little with the NPR.
(c) The separation transition process takes less than 5 ms.
(d) The instability of the shock waves always accompanies the transition of the separation patterns. The strength of the separation shock changes and disappears. Subsequently, a new separation shock appears during the transition process of the separation patterns.
(e) The NPRs of the separation pattern transition are different in the startup and the shutdown processes. This difference produces a hysteresis effect.

Acknowledgments We would like to acknowledge the support of National Natural Science Foundation of China (No. 90916023), Funding of Jiangsu Innovation Program for Graduate Education (No. CXZZ13_0177) and Fundamental Research Funds for the Central Universities.

References

1. Hiraiwa, T., Ito, K., Sato, S., Ueda, S., Tani, K., Tomioka, S., Kanda, T.: Recent progress in scramjet/combined cycle engines at JAXA, Kakuda space center. Acta Astronaut. **63**(5–6), 565–574 (2008)
2. Kanda, T., Tani, K., Kudo, K.: Conceptual study of a rocket–ramjet combined-cycle engine for an aerospace plane. J. Propuls. Power **23**(2), 301–309 (2007)
3. Kouchi, T., Keobayashi, K., Kudo, K., Murakami, A., Kato, K., Sadatake, T.: Performance of a RBCC combustor operating in ramjet mode. AIAA Paper 2006-4867 (2006)
4. Albertson, C.W., Emami, S., Trexler, C.A.: Mach 4 test results of a dual-flowpath, turbine based combined cycle inlet. AIAA Paper 2006-8138 (2006)
5. Herrman, H., Rick, H.: Propulsion aspects of hypersonic turboramjet-engines with special emphasis on nozzle/afterbody integration. ASME Paper 91-GT-395 (1991)
6. Gamble, E., Haid, D.: Improving off-design nozzle performance using fluidic injection. AIAA Paper 2004-1206 (2004)
7. Gamble, E.J., DeFrancesco, R., Haid, D., Buckwalter, D.: Fluidic nozzle to improve transonic pitch and thrust performance of hypersonic vehicle. AIAA Paper 2005-3501 (2005)
8. Verma, S.B.: Shock unsteadiness in a thrust optimized parabolic nozzle. Shock Waves **19**(3), 193–212 (2009)
9. Tomita, T., Takahashi, M., Sasaki, M., Sakamoto, H., Takahashi, M., Tamura, H.: Experimental evaluation of side-loads in LE-7A prototype engine nozzle. Shock Waves **19**(3), 213–228 (2009)
10. Nasuti, F., Onofri, M.: Shock structure in separated nozzle flows. Shock Waves **19**(3), 229–237 (2009)
11. Hadjadj, A., Onofri, M.: Nozzle flow separation. Shock Waves **19**(3), 163–169 (2009)
12. Bourgoing, A., Reijasse, P.: Experimental analysis of unsteady separated flows in a supersonic planar nozzle. Shock Waves **14**(4), 251–258 (2005)
13. Papamoschou, D., Zill, A., Johnson, A.: Supersonic flow separation in planar nozzles. Shock Waves **19**, 171–183 (2009)
14. Frey, M., Hagemann, G.: Flow separation and side-loads in rocket nozzles. AIAA Paper 99-2815 (1999)
15. Nave, L.H., Coffey, G.A.: Sea level side loads in high-area-ratio rocket engines. AIAA Paper 73-1284 (1973)
16. Watanabe, Y., Sakazume, N., Tsuboi, M.: LE-7A engine nozzle problems during the transient operations. AIAA Paper 2002-3841 (2002)
17. Yu, Y., Xu, J.L., Mo, J.W., Wang, M.T.: Numerical investigation of separation pattern and separation pattern transition in overexpanded single expansion ramp nozzle. Aeronaut. J. **118**(1202), 399–424 (2014)
18. Mo, J.W., Xu, J.L., Zhang, L.H.: Design and experimental study of an over-under TBCC exhaust system. J. Eng. Gas Turb. Power **136**(1), 014501 (2014)
19. Ben-Dor, G.: Shock Wave Reflection Phenomena, 2nd edn. Springer, Heidelberg (2007)